scientific reports

Check for updates

OPEN

Presentation and characterisation of the ALBA micro8 system for targeted hyperthermia in small animal research

J. A. Groen[1,2,3], R. Zweije[1], J. Sijbrands[1], E. M. Scutigliani[3,4], H. W. M. van Laarhoven[2,3,5], M. F. Bijlsma[2,6], J. Crezee[1,2,3] & H. P. Kok[1,2,3]✉

Preclinical therapeutic hyperthermia cancer research provides essential insight into biological and physiological effects, therapeutic impacts, and treatment-strategy optimisation. As hyperthermia triggers both local and systemic effects, orthotopic tumour models are required for translational research. Preclinical hyperthermia devices capable of adequately heating orthotopic tumours were previously unavailable. To address this, a phased-array electromagnetic heating system was developed with eight 1.66 GHz waveguide antennas. This study evaluates its ability to generate and control a heating focus in phantoms, and examines its correlation with numerical predictions. Focus size and power-steering capabilities were assessed by E-field scanning for a central focus and a 10 mm shifted focus. Temperature distributions were measured in muscle-equivalent phantoms (d = 40 mm, l = 90 mm) for central and 7.5 mm shifted foci. Results were compared with simulations by Plan2Heat, a dedicated treatment planning package for hyperthermia applications. The system successfully generated confined power foci with a radial diameter of 8 mm (FWHM). The measured temperature focus was 22 × 25 mm. The simulation-predicted focus location matched measurements within 1 mm for both power and temperature. The system generates a confined, controllable, and predictable heat focus suitable for deep targets, required for effective preclinical hyperthermia research into clinically relevant biological and physiological effects. Future work should focus on validation in mice.

Keywords Preclinical hyperthermia, Mouse heating, Phased-array electromagnetic heating, Focus control, E-field scanning, Split phantom, Simulation validation

Hyperthermia, a treatment modality in which tumours are heated to a temperature between 40 and 44 °C for about an hour, aims to amplify the efficacy of radiotherapy and chemotherapy. The combined use of these treatments increases tumour cell-killing without a concomitant increase in significant normal tissue toxicity[1]. Hyperthermia showed enhanced treatment outcomes for multiple tumour types, including cervical, rectal, and bladder cancers as well as melanomas, sarcomas, and recurrent breast tumours[2–6].

Extensive experimental research has addressed the biological mechanisms responsible for the increased effectiveness of treatments combined with hyperthermia. Several direct and indirect hyperthermia effects have been identified including inhibition of DNA-damage repair, increase of perfusion, re-oxygenation, killing of hypoxic tumour cells, influencing macromolecular delivery, triggering a heat shock response and stimulating the immune system[7–11]. However, these mechanisms are activated at varying temperature levels and not all fundamental mechanisms, as well as their relative importance, are fully understood yet. As a result, hyperthermia treatment protocols vary among institutes[12–14]. Treatment parameters such as the ideal thermal dose and the

[1]Radiation Oncology, Amsterdam UMC, location University of Amsterdam, Amsterdam, The Netherlands. [2]Cancer Center Amsterdam, Cancer biology and immunology, Amsterdam, The Netherlands. [3]Cancer Center Amsterdam, Treatment and quality of life, Amsterdam, The Netherlands. [4]Medical Biology, Amsterdam UMC, location University of Amsterdam, Amsterdam, The Netherlands. [5]Medical Oncology, Amsterdam UMC, location University of Amsterdam, Amsterdam, The Netherlands. [6]Center for Experimental and Molecular Medicine, Laboratory of Experimental Oncology and Radiobiology, Amsterdam UMC, location University of Amsterdam, Amsterdam, The Netherlands. ✉email: h.p.kok@amsterdamumc.nl

most effective time interval between hyperthermia and other modalities – radiotherapy or chemotherapy – are still topics of debate[7,15–18].

Consequently, there is a need for more preclinical research to improve our understanding of the hyperthermia working mechanisms and translating that into optimal treatment protocols. Preclinical models allow exploring various temperature ranges, durations, and combinations of modalities in a controlled and reproducible experimental setting. However, successful translation of preclinical results into viable treatment protocols requires that the preclinical model is representative for the clinical setting. Hyperthermic effects include effects at the macroscopic level that are not captured by subcutaneous graft tumour models, e.g., alteration of the tumour microenvironment. Therefore, orthotopic or genetically engineered (GE) tumour models are preferably used. The latter offering accurate representation of in vivo tumour biology, complete with a functional immune system. The anatomical tumour location in these models may be deep within the organism, requiring dedicated heating systems for treating the same way as humans are treated.

There are multiple techniques available for inducing hyperthermia in small animals[19]. Superficial tumours can be heated using methods like hot water baths, cold-light sources, near-infrared lasers, focused ultrasound and capacitive heating. For deep-seated tumours, focused ultrasound, capacitive systems, and radio-frequency heating are employed[19–25]. Among these, capacitive heating is the prevalent method for deep tissue heating. This technique however falls short in accurate, targeted heating of deep-seated targets and causes a heated volume that is far too large with respect to the target volume. Focused ultrasound (FU) or phased-array radiofrequency (RF) systems are better suited for these targets due to their focusing abilities. Nevertheless, reliable delivery of a thermal dose using focused ultrasound is still challenging due to anatomical complexities such as air pockets and the need for tight feedback control[26,27].

Considering the above, radiofrequency (RF) systems are the preferred choice for reliable and representative hyperthermia in preclinical experiments on deep-seated targets. Phased array RF-systems are widely applied in the clinic as well for the same reasons. Utilising constructive interference, the energy deposition can be focused to deep-seated target areas in a reliable way. Unfortunately, scaled-down phased-array systems that are analogous to those used on humans are not readily available for small animal treatments. This limits the ability for delivering representative hyperthermia treatments in a preclinical context. To bridge this gap, the ALBA micro8 preclinical hyperthermia system, developed and produced by Med-logix SRL in Rome, Italy, has been introduced. This innovative heating system consists of eight microwave antennas operating at 1.66 GHz. The phase and amplitudes can be adjusted independently per antenna, enabling targeted tumour heating in a manner similar to human treatments. Similarly, the system contains a temperature-regulated water bolus – a water bag surrounding the mouse that provides electromagnetic coupling and skin cooling.

The ALBA micro8 system provides 16 degrees of freedom to control energy deposition (7 phases, 8 amplitudes and water bolus temperature). Controlling these parameters for focused heating in the heterogeneous anatomy of a small animal is therefore not straight-forward and requires treatment planning to predict the energy deposition and temperature distribution in tissues, also similar to clinical practice[28]. In previous work, our group has applied treatment planning tools for the ALBA micro8 to simulate heating patterns in a homogeneous phantom as well as in a realistic mouse anatomy. These theoretical results indicated that this device design should be able to realise targeted locoregional tumour heating[29]. Since the ALBA micro8 is a novel device and reliable focusing and steering at this high frequency and small scale is not trivial, a next essential step before this device can be used in pre-clinical studies is to perform real measurements. These measurements should first characterise the device using quality assurance (QA) measurements, similar to those applied for phased array devices in clinical use. Such QA measurements typically use homogeneous phantoms, because in homogeneous phantoms the basic characteristics as focus size and focusing ability are most clearly pronounced. Furthermore, it is also important to validate that treatment planning predictions can accurately predict these characteristics, since focusing in preclinical experiments will be assisted by treatment planning.

In conclusion, more representative preclinical hyperthermia research requires dedicated devices capable of well-controlled heating of deep-seated targets in small animals, comparable to clinical hyperthermia. A small-scale phased-array system, the ALBA micro8, has recently become available and theoretical evaluation of the device design by computational simulations showed excellent focusing ability. In this study, we aimed to characterise the fundamental focussing abilities and heating characteristics of the ALBA micro8, small-scale hyperthermia device using QA measurements, similar to those commonly used in QA for clinical devices[30,31]. To this end we performed E-field scans and temperature rise measurements in homogeneous phantoms with tissue-mimicking electrical conductivity. In addition, we validated treatment planning predictions of the focus size and position; a pre-requisite for future use of planning in pre-clinical experiments with the ALBA micro8.

Materials and methods

The characteristics of the 1.66 GHz eight-antenna array were assessed through a series of experiments. The electric fields (E-fields) were scanned to characterise the power-focus size and control. The consequent heat-focusing abilities of the system were assessed using muscle-equivalent split phantoms. Experimental data were compared with simulations, evaluating the focus size (i.e. full width half maximum) and the focus location (i.e. location of the peak).

ALBA micro8

The ALBA micro8 small animal heating system is a phased-array waveguide ring with a bore of 50 mm, enabling 2D focus control in the transversal midplane. The antennas operate at 1.66 GHz, a frequency selected to allow for a well-defined focal zone, combined with adequate steering properties to target the heating to the desired location without introducing significant hot spots outside the target region. At this frequency, the resulting wavelength is about 20 mm in deionised water (25 mm in muscle). The waveguides are filled with deionised

water and can operate at 5 W each. The space between the antennas and the animal is filled with a water bag (bolus) containing deionised water. This bolus couples the electromagnetic fields to the animal and cools the skin.

Number of antennas

A controllable focus can already be created using only 4 antennas, similar to the 4 antennas in the clinical ALBA 4D system (Medlogix, Rome Italy). However, because of the relatively short wavelength of 1.66 GHz, with 4 antennas smaller sub-foci will arise in addition to the main focus. These sub-foci likely cause unwanted heating outside the tumour region. A lower frequency would increase the wavelength and thereby reduce these sub-foci, but this would also increases the size of the main focus and, most important, this would reduce small scale steering capabilities, thus potentially limiting research applications[32–34]. To enable a wide variety of preclinical studies to investigate targeted and heterogeneous heating while still maintaining the robustness of the waveguide ring, the frequency was maintained at 1.66 GHz and the number of antennas extended to eight antennas. Simulation results of an antenna ring in deionised water with four and eight antennas are visualised in Fig. 1a, showing a better focused heating zone with 8 waveguides. The realised 8-antenna array is presented in Fig. 1b. Phases of all configurations can be found in Table 1.

E-Field scans

The power focusing and control capabilities of the 8-waveguide phased array were assessed using E-field scans and compared with simulations. The scans were performed with the antennas submerged in deionised water. The fields were scanned by moving a probe through the field in a stepwise manner using a Cartesian coordinate robot. The E-field probe consisted of a passive monopole antenna of approximately 2.5 mm (1/8 λ) in length and 0.5 mm in diameter, connected to a 1 mm diameter coax cable. The probe was oriented in the direction of the dominant E-field component (i.e. Z-direction). The probe size was sufficiently small to avoid significant disturbance in (relative) field measurements. Since the X and Y field components are negligible in the central measurement plane, only the Z-component was measured. At the start of measurement, the probe was calibrated against the forward signal on the feeding cable. At each step, power was measured (±0.2 dB) using a Vector Network Analyzer (VNA) (Model ZNC 3, Rhode&Schwarz, Munich, Germany), resulting in a relative power pattern. A schematic drawing of the experimental setup is visualised in Fig. 2a.

First, the field pattern of a single waveguide antenna was scanned to get a detailed view of the field distribution generated by the individual antennas. For this case, the antenna was moved using the robot instead of the probe. A total grid of $60 \times 60 \times 60$ mm^3 was scanned in front of the waveguide antenna with a resolution of $1 \times 1 \times 1$ mm^3. Water temperature during the single antenna scans was about 25 °C. Next, the field distribution generated by the full eight antenna array was scanned. This was done for two sets of phase settings: (i) Centre focus (all phases set to zero) and (ii) phases optimised based on SAR-ratio optimisation for focusing on a shifted target at (X, Y) = (−10, 0) mm from the centre. The scans of the antenna array covered the radial plane, with a diameter of 42 mm (within the 50 mm bore) at a resolution of 3×3 mm^2. This represents the region of interest enclosed by the water bolus. Values between measurement points were determined by cubic interpolation. Water temperature during the antenna array scans was about 21 °C. Phases of all antenna configurations can be found in Table 1.

Temperature distribution measurement

Thermal focus and focus-control characteristics were evaluated using homogeneous phantoms with electrical conductivity similar to that of muscle. The antenna array was placed in vertical orientation in a container to allow quick handling of the phantom after power-off. Similar to the field scans, the container was filled with deionised water. A schematic drawing of the split phantom setup is shown in Fig. 2b.

The agar-agar gel phantoms were made by mixing distilled water with 50 g/L agar-agar and 4.0 g/L of NaCl to adjust the electrical conductivity such that it represents the conductivity of muscle tissue at 1.66 GHz. The resulting permittivity is somewhat higher than for muscle tissue. However, this minimally affects the wavelength and thus allows for realistic evaluation of power steering capabilities of the ALBA micro8. The mixture was stirred and heated until thickened (but not boiling), then poured into moulds to form cylindrical phantoms, each 40 mm in diameter and 90 mm in height. The dielectric properties of phantoms created following this recipe were measured using a Dielectric Assessment Kit (DAK) 12 probe (4 MHz–3 GHz) from SPEAG (Zurich, Switzerland) and are shown in Table 2.

Phantoms were positioned inside the bore of the system and heated for 10 min at 7.8 W output power. After heating, the phantom was removed and cut in half, either axially or radially. A thermal image was then taken of the cut-surface midplane using a FLIR b60 infrared camera (Wilsonville, OR, USA) to visualise the temperature distribution. The camera has a documented accuracy of ±2 °C and thermal sensitivity (N.E.T.D) < 0.08 °C at 25 °C. The emissivity was set to 1. The camera was calibrated using a black body source (Hyperion R982) on temperatures between 20 and 40 °C with 0.5 °C steps.

The time from power-off to thermal photograph was kept within 10 s to avoid significant temperature conduction washout. Slicing was performed within 0.5 s. The experiment was performed with antenna settings for a centre focus (all phases set to zero) and for a shifted focus. The focus shift was chosen at (X, Y) = (−7.5, 0) mm from the centre instead of −10 mm. Since the thermal focus is typically wider than the SAR focus, a −10 mm shift would result in a focus near the boundary of the phantom. This smaller shift will yield a better defined thermal focus, suitable for characterising deep heating steering capabilities. Phase-settings for the shifted focus were based on SAR-ratio optimisation. The ambient temperature during the experiments was 21 °C. A photograph of the split-phantom setup is shown in Fig. 2b. The phase configurations of all antennas can be found in Table 1.

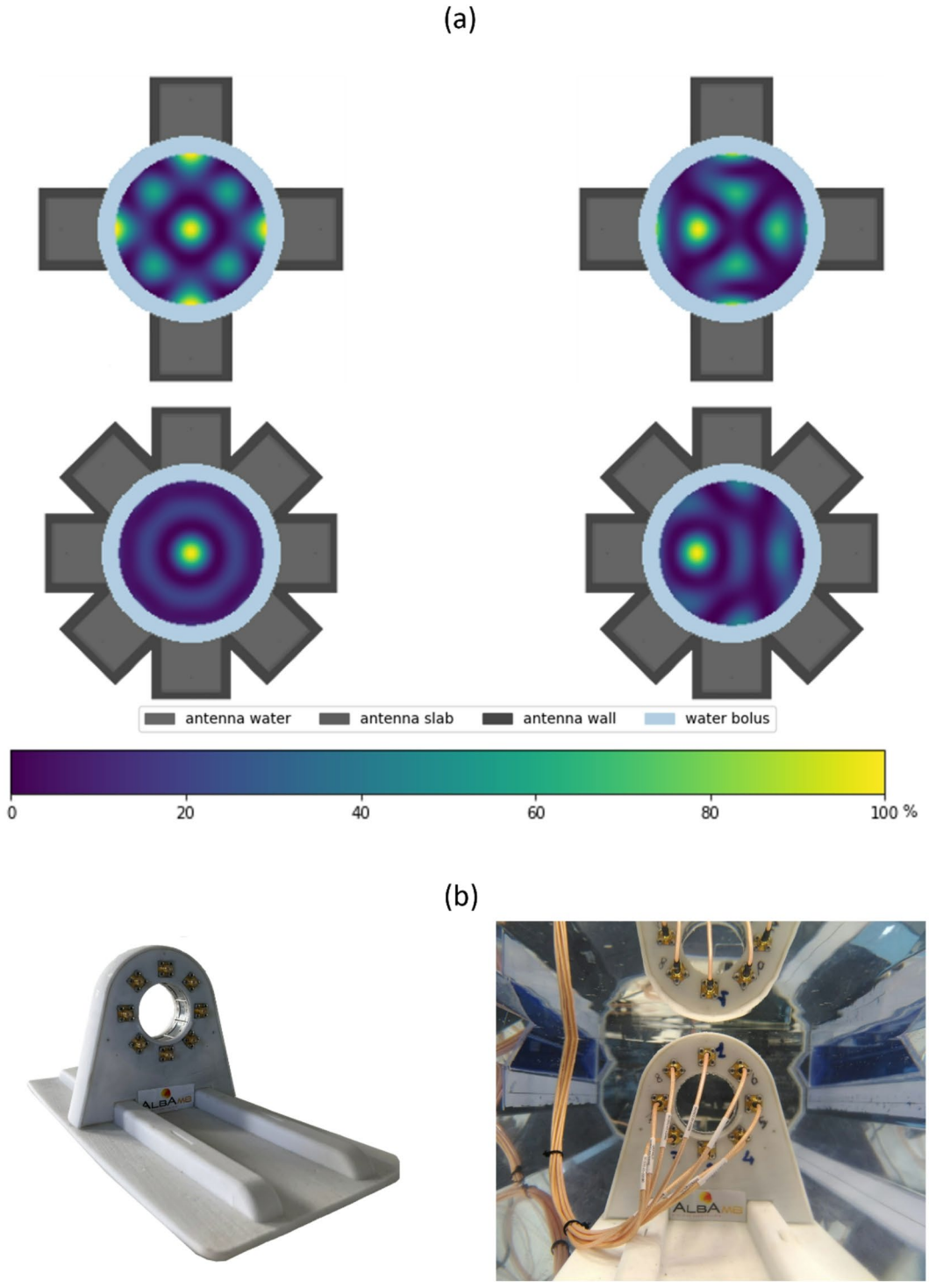

Fig. 1. Power density distribution simulations of 1.66 GHz waveguide antenna arrays of four antennas (a, top) versus eight antennas (a, bottom) and the realised system (b) with a rear view of the system submerged in de-ionised water as used in E-field scanning experiments (as illustrated in Fig. 2a). Phase settings used were all zero for the centre focus (a, left) or optimised based on SAR-ratio optimisation for a target shifted 10 mm from the centre (a, right). Phase settings can be found in Table 1. All plots are individually normalised on the maximum value of the focus. Eight antennas allow for better focusing of power, while lowering the relative magnitude of the sub foci.

antenna	Centre focus	focus shift (4-antennas)	focus shift 10 mm* (8-antennas)	focus shift 7.5 mm** (8-antennas)
top	0	0	0	0
top right	0	-	128	134
right	0	128	152	21
bottom right	0	-	128	134
bottom	0	0	0	0
bottom left	0	-	−141	−113
left	0	178	165	−155
top left	0	-	−141	−113

Table 1. Phase settings (°) for the 1.66 GHz antenna array. Settings were optimised based on SAR-ratio optimisation. *The 10 mm focus shift was optimized for the E-field scan (no phantom present). **The 7.5 mm focus shift was optimized for split-phantom heating (shift inside the phantom).

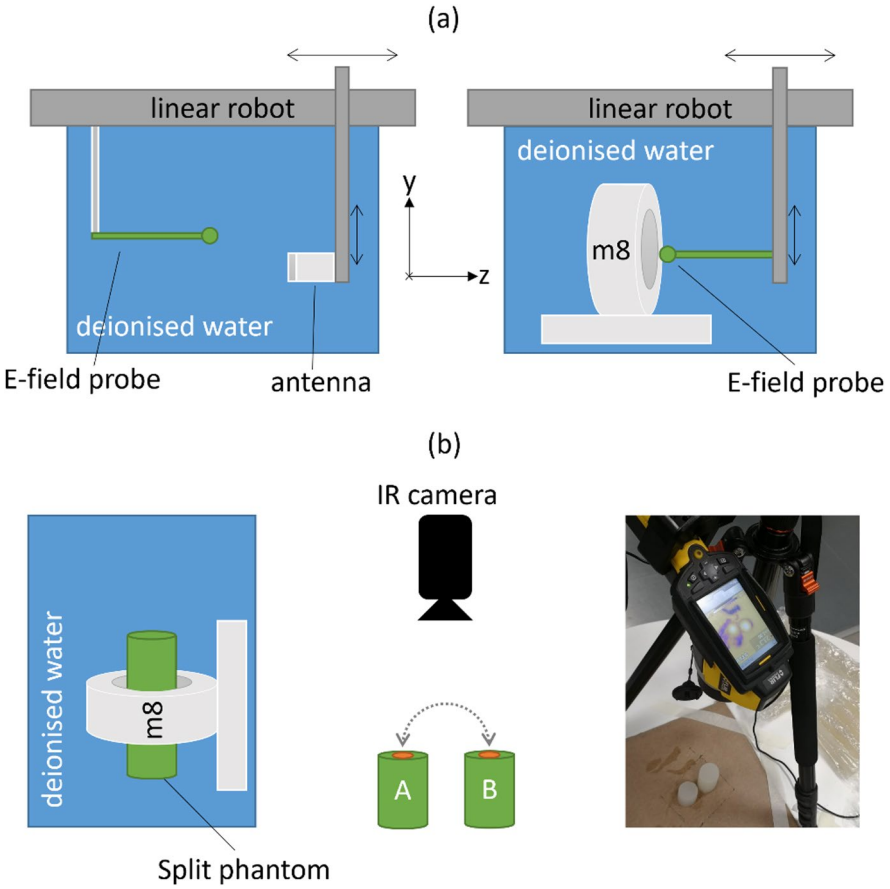

Fig. 2. Illustration of the measurement setups containing the E-field scan setup (**a**) and the split phantom setup (**b**). Experiments were performed within a container filled with deionised water. During the E-field scans (a), a Cartesian coordinate robot (linear robot) is used to position the antenna (single antenna scan) or the E-field probe (antenna-array scan). For the single antenna scan (a, left), the field in front of the antenna was scanned. For the ALBA micro8 (side view, m8 in figure) scan (a, right), the xy-plane at the centre of the bore was scanned. A scan was made by moving the probe while repeatedly taking power measurements. During the split phantom measurements (b), heating of the agar phantom was performed within the container filled with deionised water. The ALBA micro8 (side view, m8 in figure) was placed vertically to allow quick handling of the phantom. After 10 min of heating, the phantom was sliced in halves resulting in parts A and B, and the cut-surface was imaged using an infrared (IR) camera (FLIR b60, Wilsonville, ON, USA).

	$\sigma \left[S\,m^{-1}\right]$	ϵ_r	$\rho \left[kg\,m^{-3}\right]$	$C_p \left[J\,kg^{-1}K^{-1}\right]$	$k \left[W m^{-1}K^{-1}\right]$
Agar gel	1.33	75	1000	4180*	0.6*
Deionised water	0.63	79	1000	4180	0.6
Muscle**	1.27	54	1081	3421	0.5

Table 2. Electrical and thermal properties of deionised water and 50 g/L agar gel with 4.0 g/L NaCl at a temperature of 21 °C. The dielectric properties were measured using a dielectric assessment kit (DAK) 12 probe (4 MHz–3 GHz) from SPEAG (Zurich, Switzerland). *Based on deionised water at room temperature. **Data obtained from the IT'IS database[35].

Computational modelling

Simulations were performed using the Finite Difference Time Domain (FDTD) treatment planning software, Plan2Heat (Amsterdam UMC, the Netherlands)[36]. The system was modelled by individually modelling each of the eight waveguides as a rectangular box with a depth of 16 mm and an aperture of 16 × 10 mm. The electromagnetic source is placed between the choke and the wall. The system was modelled to be submerged inside deionised water. The total modelled volume was 100 × 100 × 100 mm^3. All simulations were performed at a resolution of 0.4 × 0.4 × 0.4 mm^3, which is about λ/50; yielding a substantially finer grid compared to the minimally required λ/10 - λ/15 for FDTD calculations[37]. The E-field distribution resulting from each individual waveguide is calculated separately with unit amplitude and zero phase, with non-radiating waveguides terminated by the theoretical characteristic impedance of 50 Ω.

The antenna settings for the shifted focus were found based on SAR_{ratio} optimisation:

$$SAR_{ratio} = \frac{mean(SAR_{rest\ of\ the\ phantom})}{mean(SAR_{target})} \tag{1}$$

with $SAR\ \left(W\ kg^{-1}\right)$ at voxel i being the point SAR, calculated as:

$$SAR_i = \frac{1}{2}\frac{\sigma_i |E_i|^2}{\rho_i} \tag{2}$$

where $\sigma\ \left(S\ m^{-1}\right)$ is the electrical conductivity, $\rho\ \left(kg\,m^{-3}\right)$ is the density, and $E\left(V\,m^{-1}\right)$ is the total electric field. The target was defined by a spherical mask of 10 mm in diameter.

Temperature distributions were predicted by solving Pennes' bioheat equation[38]. Since there are no biological tissues involved in this study, the equation results in the basic heat-transfer equation:

$$c\rho\frac{\partial T}{\partial t} = \nabla \cdot (k\,\nabla T) + P \tag{3}$$

with c representing the specific heat capacity $\left(J\,kg^{-1}\circ C^{-1}\right)$ and $k\left(W\,m^{-1}\circ C^{-1}\right)$ is the thermal conductivity. The power density deposited by the heating system is represented by P ($W\,m^{-3}$). A Dirichlet boundary condition was used at the border of the computational domain.

Evaluation of treatment planning

To evaluate whether the treatment planning software can accurately predict the performance of the antenna array, the predicted focus size and location were compared with the obtained results from the E-field and split phantom experiments. The focus size was determined using 1D profiles and measuring the full width half maximum (FWHM). The location of the focus was determined by the peak location. A direct comparison between measurements and simulations was performed by evaluating the Z-component of the E-field and the temperature resulting from the total E-field.

Results

E-field scans

E-field scans in deionised water were used to characterise the electric field distribution of the system and this was found to correspond well with numerical predictions. The measured field of a single 1.66 GHz waveguide antenna showed a forward directed field, diminishing in a concentric manner at larger distances from the antenna. The contour plots (Fig. 3a) illustrate the spatial E-field distribution in the transversal mid-plane in decibels (dB) for both measured and simulated data. The measured and simulated electric field (E-field) distributions were markedly similar, though those of the simulated field are slightly more elliptical shaped, compared to the more circular lines in the measured data. The profiles in Fig. 3b show the measured and simulated E-field magnitudes in dB as a function of distance from the aperture, which further supports the agreement between simulation and measurement. Both the measurement and simulation curves exhibit similar rate of decay in E-field intensity with increasing distance from the centre. The simulated penetration depth (i.e., the depth at which the power has reduced by 50%) was measured at about 5 mm (4 mm simulated).

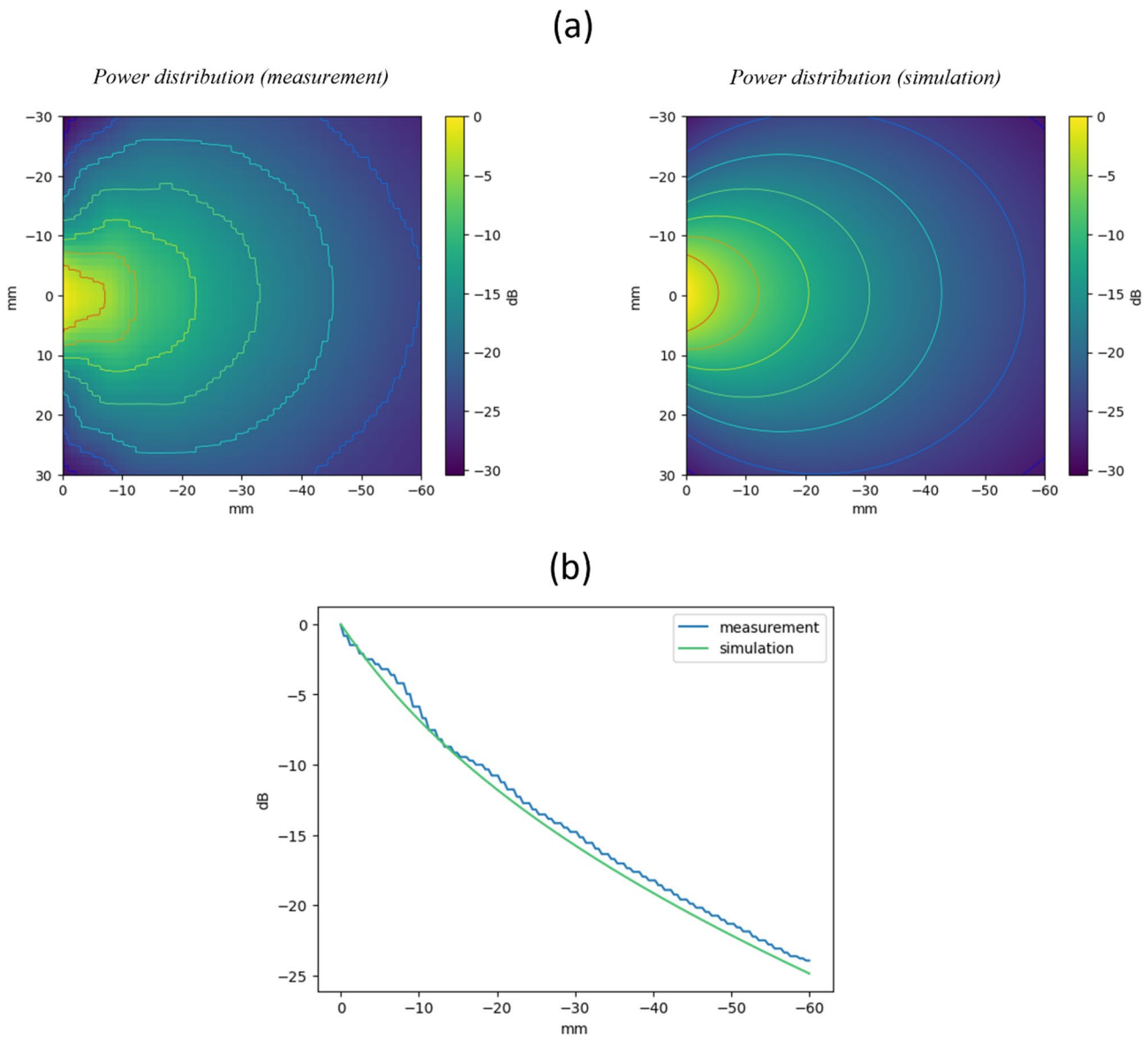

Fig. 3. Comparison of the electric field scan in deionised water (measured in power) with simulations. (**a**) Contour plots of the E-field in decibels (dB), with measurements shown on the left and simulations on the right, both displaying a similar field distribution pattern. (**b**) The corresponding E-field magnitudes in dB as a function of distance (mm) from the antenna, indicating a close agreement between measured and simulated values. The penetration depth (50% power) was measured at about 5 mm (4 mm simulated).

E-field scans of the entire antenna array showed that a confined focus could be generated and steered with highly predictable accuracy. Figure 4 presents a comparison between the electric field (E-field) scans and corresponding simulations of the entire antenna array for the two target locations (centre focus and − 10 mm horizontal shift). In the centre focus configuration, the E-field demonstrates a symmetrical distribution, with a pronounced central peak and a concentric ring. The measurement and simulation results were almost identical. Both measured and simulated peak size (FWHM) was ~ 8 mm. The location of the measured peak was within 0.5 mm from the centre.

For the shifted focus configuration, the measured peak shift was exactly 10 mm, as predicted by the simulations, again with a deviation of less than 0.5 mm. The measured focus was slightly more stretched along the y-axis compared to the simulation, with the measured FWHM 10 mm against a simulated value of 8 mm. Small deviations can be observed between the measured and simulated interference pattern outside the focal zone, where the field values are very low. Secondary E-field peaks are observed close to the boundary of the measurement domain. Since in practical applications the surrounding water will be kept a at a constant temperature for skin cooling, similar to locoregional hyperthermia for human applications, these secondary peaks will not induce high temperatures due to the bolus cooling effect, and will thus not affect the performance of the device.

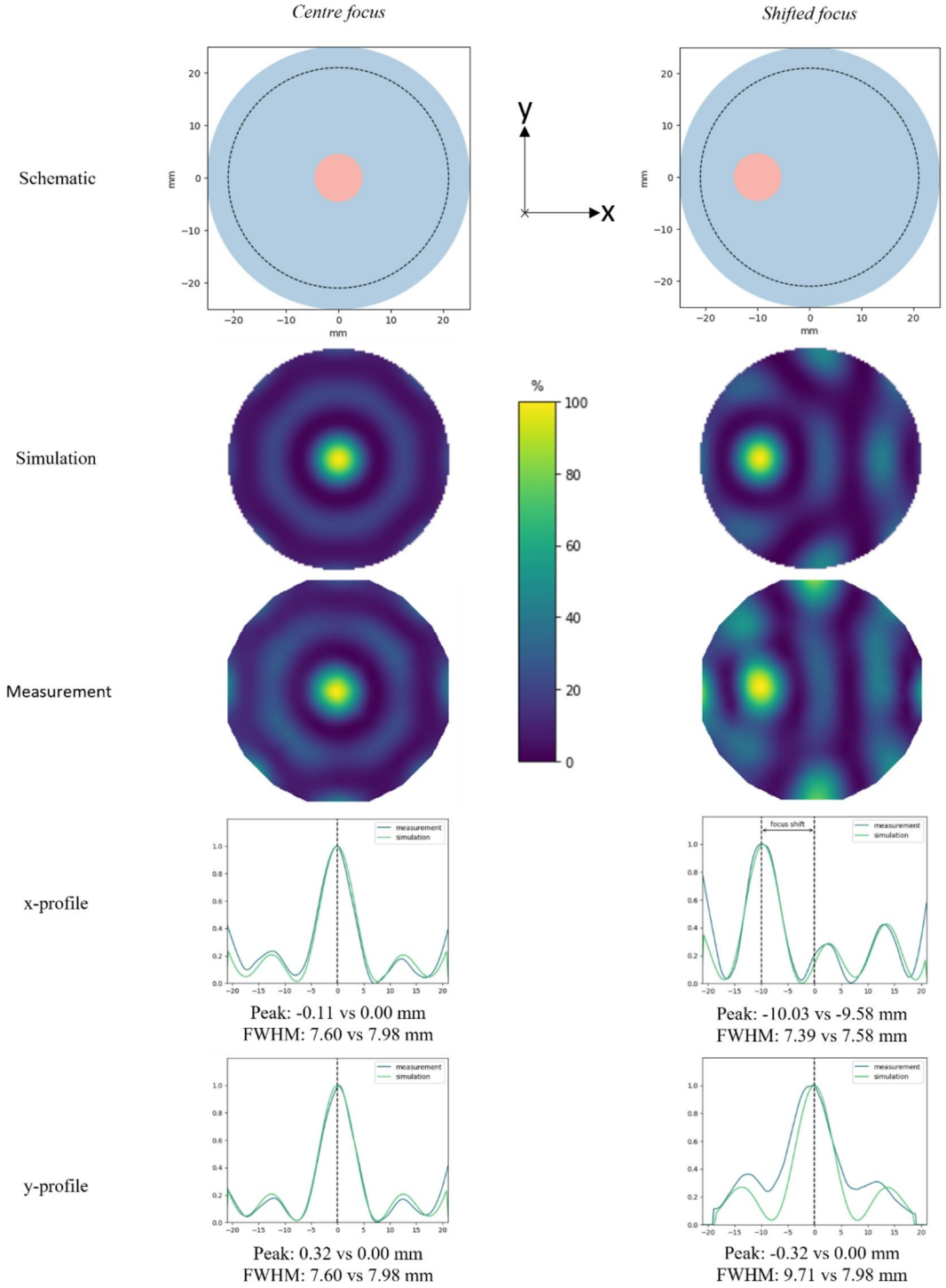

Fig. 4. Comparison between E-field scan and corresponding simulation with the ALBA micro8 antenna array submerged in deionised water. Scans were performed in the transversal mid-plane for a focus in the centre (left side) and for a focus 10 mm shifted (right side). Focus location is visualised in red in the schematic plots. Horizontal (x) and vertical (y) profiles were extracted through the peak of the E-field to assess spatial agreement between measurement and simulation.

Temperature distribution measurements

Phantom measurements characterised the heat focus and showed that confined heating was possible and steerable with high accuracy. Figure 5a presents infrared (IR) photographs of the split-phantom experiments, showing the thermal distribution for different focus configurations of the ALBA micro8 antenna array. The heat focus was clearly visible, with a measured ellipsoidal shape (X×Z) of about 22 × 25 mm. This closely matched simulation

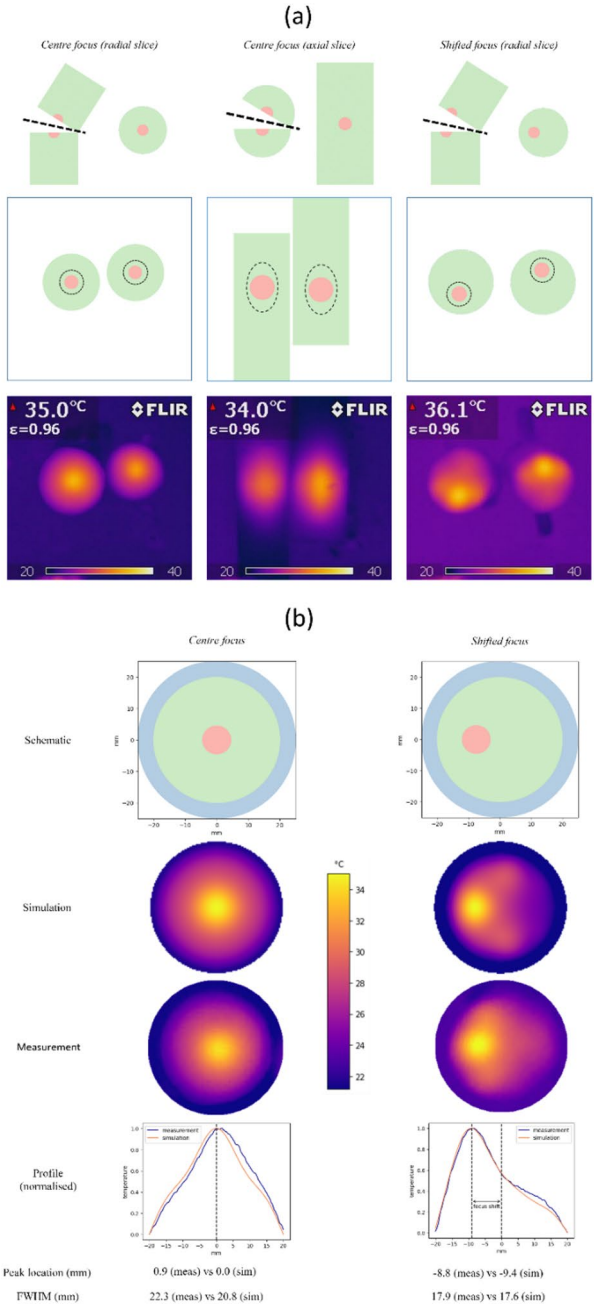

Fig. 5. Measurements versus simulations of split-phantom experiments. The cylindrical phantoms, with a diameter of 40 mm, were heated for 10 min at a total power of 7.8 watts. The phase offsets were configured for either a central focus or a shifted power focus (7.5 mm from the centre). The phantoms were then sliced either radially or axially through the midplanes, and IR photographs were taken within 10 s of power-off to capture the heat distribution (a). Slight asymmetries between the halves are explained by small imperfections during slicing (a). In the comparison shown in (b), the images represent radial slices; both focus size (error < 1.5 mm) and location (error < 1 mm) were accurately predicted by the simulations.

results, which predicted an ellipsoid of X×Z=(Y×Z) = 21 × 28 mm. The maximum recorded temperature rise after the 10 min heating was about 15 °C. A comparison of the measured temperature distributions and the simulated distributions is found in Fig. 5b, highlighting both central and shifted focus configurations. The diameter of the central heat focus was measured at 22 mm, compared to 21 mm in simulation. This size decreased slightly for the shifted focus configuration, measuring 18 mm (both measured and simulated). In the shifted focus configuration (right, radial slice), the IR photograph showed a focus displacement of 8.8 mm, which compared well to the simulated displacement of 9.4 mm.

A summary of all quantitative results is shown in Table 3. The position of the focus was accurately predicted by the simulation within 1 mm. The size of the focus was predicted within 1.5 mm.

	Measured	simulated
Penetration depth (single waveguide)	5 mm	4 mm
E-field centre focus		
Focus size (FWHM)	7.6 mm	8.0 mm
Focus location	−0.1 mm	0.0 mm
E-field shifted focus		
Focus size (FWHM)	7.4 mm	7.6 mm
Focus location	−10.0 mm	−9.6 mm
Thermal centre focus		
Focus size (FWHM)	22.3 mm	20.8 mm
Focus location	0.9 mm	0.0 mm
Thermal shifted focus		
Focus size (FWHM)	17.9 mm	17.6 mm
Focus location	−8.8 mm	−9.4 mm

Table 3. Summary of quantitative results, including penetration depth and characteristics (size and location) of both central and shifted foci in the E-field and temperature distributions. The measured results are compared to predicted values and show excellent agreement.

Discussion

The study focuses on the ALBA micro8 system, a novel device designed to deliver precise, targeted heating in small animal models, similar to human locoregional hyperthermia. This work is the first to experimentally validate its performance, which is essential to ensure reliable preclinical hyperthermia studies using this device, aiding in the translation of preclinical findings into effective clinical protocols and improve hyperthermia as modality.

The power control and heating abilities of the ALBA micro8 were characterised by performing two series of experiments. E-field scans showed that the system can create a confined power focus and control its location within 1 mm accuracy compared with treatment planning predictions. These capabilities translate into a controllable heat focus that was evaluated using tissue-mimicking split phantoms, where the measured and simulated peak location also matched within 1 mm. Being able to create a localised heating focus of which its size and location can be accurately predicted enables well-controlled deep, targeted heating in a preclinical setting. The ALBA micro8 will therefore serve its purpose as a small animal phased-array hyperthermia device.

All experiments in this study were performed with the antenna ring submerged in deionised water. This enabled to perform scan measurements in a large area, i.e. 42 mm diameter within the 50 mm bore. When using a physical phantom, e.g. an open cylinder with 30–40 cm diameter enclosed by a water bolus, the physical measurement volume would be severely limited due to phantom border and the dimensions of the E-field probe. Furthermore, this open water bolus set-up also ensured optimal coupling between the antennas and the split phantom, ensuring that the fundamental performance of the antenna-ring is evaluated. The results of this study can be generalised to the use with a true physical water bolus provided that good contact between the water bolus and the phantom/animal is ensured to avoid air pockets, as these can cause reflections. In practical applications, ensuring optimal contact when using a closed bolus could require significant water pressure, potentially yielding discomfort, or maybe even hazard, to the animal. Therefore, using an open water bolus in future in vivo applications may also have significant advantages; this will be subject of further research.

Figure 4 clearly showed the ability of the ALBA micro8 to create a confined predictable focus and control its location. Both the focus size and its location could be predicted within 1 mm accuracy. Some small deviations between measurements and simulations could be observed for the situation with a shifted power focus. Possible contributions to this difference include the imperfect simulation of the waveguides (as seen in Fig. 3, single antenna scan), uncertainty in the dielectric properties of the measurement medium, imperfections in phase/amplitude calibration, phase/amplitude lock issues, interference of the measurement sensor, antenna crosstalk influencing the control circuit, and E-field scan resolution (3×3 mm). Nevertheless, since focus size and location could be accurately predicted and these deviations are in areas outside the focal zone with relatively low field values, there will be no significant impact on practical performance.

The maximum temperatures measured with the infrared camera were up to 36 °C, i.e., a 15 °C rise in 10 min. This is significantly faster than the minimum temperature increase of 6 °C in 10 min, typically required in QA for human locoregional hyperthermia to ensure achieving therapeutic temperatures during treatments. This indicates that the ALBA micro8 has sufficient power to mimic clinical locoregional hyperthermia. In clinical locoregional hyperthermia treatments, with active heat removal by blood perfusion, the warm-up time is typically about 30 min, after which the real 1 h treatment starts. It would be possible to mimic a clinical treatment, including warm-up time, by adjusting the output power. Similar to clinical hyperthermia treatments, preclinical experiments will always be guided by invasive measurements in the target location. Treatment planning will be used to determine phase-amplitude settings to focus the heating to the desired target location; during treatment the exact temperature level will be controlled by on-line thermometry feedback. During our experiments, no differences in system behavior were observed when varying the output power.

Measurements and simulations showed a difference of 1 °C in peak temperature. Deviations between measurement and simulation could possibly occur from increasing room temperature, imperfect slicing, varying time intervals between power off and slicing and the impact of slicing itself. The latter three effects could also help to explain the remaining inaccuracies in heat focus size (± 2 mm) and location (± 1 mm). Another uncertainty comes from the emissivity, which was set to 1 and is probably slightly too high. However, since the agar mixture is ~ 95% water, emissivity is likely to be close to 1. This uncertainty in emissivity might also have contributed to the (small) discrepancy between measurements and simulations, but the impact is likely within the tolerance of the camera itself. Nevertheless, it should be noted that the observed 1 °C difference is within the documented accuracy for absolute values of the camera (± 2 °C), and will not limit the use of treatment planning in pre-clinical experiments, since preclinical experiments will be guided by temperature measurements.

A limitation of this study is that each experiment was performed only once, which is due to the fact that the measurements were rather time-consuming, and many different tests had to be performed. However, the study contains several different experiments, including also shifted focus and thermal distribution evaluation. Furthermore, the simulation predictions also showed a good match with all the different experimental results, which were achieved for very different system settings, which provides additional confidence in the accuracy of the results. Therefore, altogether these experiments cover the most relevant aspects for a characterization of the ALBA micro8. The findings of this study indicate that the ALBA micro8 system surpasses existing preclinical systems in delivering precise and localised heating for deep targets. Current preclinical systems are often designed for superficial applications or limited to specific anatomical regions such as the bladder or a leg and fail to reflect the locoregional heating used in clinical practice[19–24]. Although techniques like focused ultrasound show promise for targeted heating, they are still under development and lack the robustness needed for consistent and reproducible preclinical hyperthermia, particularly for deep-seated tumours in the abdomen and pelvis[26,27]. In contrast, the micro8 system has demonstrated the ability to provide reliable, target heating.

Future research will need to further validate the usage of this device using more complex phantoms or real anatomies. Furthermore, comprehensive in vivo studies are required that assess its safety and efficacy before the device can be used in real pre-clinical studies investigating biological hyperthermia mechanisms. In silico investigation of the performance of the ALBA micro8 in mice anatomies showed inherent robustness to various factors, including respiratory motion, changes in stomach and intestinal filling, mouse-positioning errors, and tissue property uncertainties[29]. Furthermore, simulation results showed that the exact size of the heat-focus achieved in mice can be influenced by the applied numerical optimisation strategy and bolus temperature selection. Further in vivo investigations are required to validate consistent and accurate heat delivery by the device, as well as evaluating any potential side effects or adverse reactions specific to the anatomy and physiology of (sedated) mice. Specifically, the impact of water bolus cooling requires thorough investigation because of the relatively high surface-area-to-volume ratio of mice compared to humans. Bolus temperatures should be carefully selected to achieve the desired balanced cooling effects and avoid inducing hypothermia in the animals.

Although clinical hyperthermia in combination with radiotherapy/chemotherapy is successfully applied to human patients since the 80 s, all hyperthermia working mechanisms have not been fully unravelled yet. The ALBA micro8 device has been developed to facilitate further in vivo research into biological hyperthermia mechanisms. The device was thus not designed as an exact miniature copy of a hyperthermia device for human use, but robust focusing capabilities on a small scale were most important to enable answering a wide variety of biological hyperthermia-related research questions. This way, this technology enables researchers to study in mice how targeted hyperthermia impacts tumour biology or its microenvironment. By focusing heat on specific tumour regions, researchers can dissect the cellular and molecular mechanisms underlying hyperthermia-induced tumour cell death and stress responses, leading to a better understanding of the optimal conditions for therapeutic efficacy. Additionally, this capability extends to examining the effects of heating specific organs or even parts of an organ. For instance, researchers can investigate how hyperthermia affects liver function, kidney performance, or brain activity when only a small, targeted region is heated. This precision allows for the assessment of potential systemic effects, localised tissue responses, and organ-specific toxicities, thereby providing a comprehensive understanding of the impact of hyperthermia on different biological systems. Furthermore, this approach facilitates the study of the role of hyperthermia in immune modulation, such as its ability to enhance the infiltration of immune cells into tumours or its effect on local immune responses within specific areas. This detailed level of investigation is crucial for developing effective hyperthermia protocols that maximise therapeutic benefits while minimising adverse effects (e.g. considering timing of hyperthermia with respect to other oncological treatment modalities), ultimately translating these findings into more effective clinical treatments for cancer patients.

Conclusions

First experimental characterisation of the ALBA micro8 system in phantoms indicated effective power control and heating characteristics very suitable for preclinical studies aiming at well controlled targeted heating. Through a series of experiments, the system was shown to create a confined power focus (diameter of ~ 8 mm) with precise control such that the location could be predicted within 1 mm. The system's capability to deliver precise and localised heating was validated using tissue-mimicking phantoms, in which again the location of the focal zone could be predicted within 1 mm. These findings suggest that the ALBA micro8 is well-suited for hyperthermia applications in small animals, mimicking deep-hyperthermia conditions used in human treatments. Further in vivo studies should validate the safety and efficacy of the device, particularly in terms of achieved temperature distribution and the impact on core temperature in murine anatomies. The ALBA micro8 stands as a realistic hyperthermia platform suitable for exploring very diverse biological and physiological hyperthermia effects, assessing therapeutic impacts, and refining treatment strategies for combined modality therapies on tumours.

Data availability

Data are available upon reasonable request to the corresponding author.

Received: 6 June 2025; Accepted: 23 September 2025
Published online: 29 October 2025

References

1. Datta, N. R. et al. Local hyperthermia combined with radiotherapy and-/or chemotherapy: recent advances and promises for the future, *Cancer treatment reviews*, vol. 41, no. 9, pp. 742 – 53, (2015). https://doi.org/10.1016/j.ctrv.2015.05.009
2. Overgaard, J. et al. Randomised trial of hyperthermia as adjuvant to radiotherapy for recurrent or metastatic malignant melanoma. *Lancet* **345** (8949), 540–543. https://doi.org/10.1016/S0140-6736(95)90463-8 (1995).
3. Vernon, C. C. et al. Radiotherapy with or without hyperthermia in the treatment of superficial localized breast cancer: results from five randomized controlled trials. International collaborative hyperthermia group. *Int. J. Radiat. Oncol. Biol. Phys.* **4** (35), 731–744. https://doi.org/10.1016/0360-3016(96)00154-x (1996).
4. van der Zee, J. et al. Comparison of radiotherapy alone with radiotherapy plus hyperthermia in locally advanced pelvic tumours: a prospective, randomised, multicentre trial. Dutch Deep Hyperthermia Group, *Lancet*, vol. 355, no. 9210, pp. 1119-25, (2000). https://doi.org/10.1016/s0140-6736(00)02059-6
5. Issels, R. D. et al. Neo-adjuvant chemotherapy alone or with regional hyperthermia for localised high-risk soft-tissue sarcoma: a randomised phase 3 multicentre study, *Lancet Oncol*, vol. 11, no. 6, pp. 561 – 70, (2010). https://doi.org/10.1016/S1470-2045(10)70071-1
6. Longo, T. A. et al. A systematic review of regional hyperthermia therapy in bladder cancer. *Int. J. Hyperth.* **32** (4), 381–389. https://doi.org/10.3109/02656736.2016.1157903 (2016).
7. Dewhirst, M. W., Vujaskovic, Z., Jones, E. & Thrall, D. Re-setting the biologic rationale for thermal therapy, *Int J Hyperthermia*, vol. 21, no. 8, pp. 779 – 90, (2005). https://doi.org/10.1080/02656730500271668
8. Oei, A. L., Vriend, L. E., Crezee, J., Franken, N. A. & Krawczyk, P. M. Effects of hyperthermia on DNA repair pathways: one treatment to inhibit them all. *Radiat. Oncol.* **10**, 165. https://doi.org/10.1186/s13014-015-0462-0 (2015).
9. Mahmood, J. et al. Immunotherapy, Radiotherapy, and hyperthermia: A combined therapeutic approach in pancreatic cancer treatment. *Cancers (Basel)*. **10** (12). https://doi.org/10.3390/cancers10120469 (2018).
10. Scutigliani, E. M., Lobo-Cerna, F., Mingo Barba, S., Scheidegger, S. & Krawczyk, P. M. The effects of heat stress on the transcriptome of human cancer cells: A Meta-Analysis. *Cancers (Basel)*. **15** (1). https://doi.org/10.3390/cancers15010113 (2022).
11. Scutigliani, E. M., Liang, Y., Crezee, H., Kanaar, R. & Krawczyk, P. M. Modulating the Heat Stress Response to Improve Hyperthermia-Based Anticancer Treatments, *Cancers*, vol. 13, no. 6, p. 1243, (2021).
12. Carrapico-Seabra, C., Curto, S., Franckena, M. & van Rhoon, G. C. Avoiding pitfalls in thermal dose effect relationship studies: A review and guide forward. *Cancers (Basel)*. **14** (19). https://doi.org/10.3390/cancers14194795 (2022).
13. Ademaj, A. et al. A patterns of care analysis of hyperthermia in combination with radio(chemo)therapy or chemotherapy in European clinical centers. *Strahlenther. Onkol.* **199** (5), 436–444. https://doi.org/10.1007/s00066-022-01980-9 (2023).
14. Ademaj, A. et al. Clinical Evidence for Thermometric Parameters to Guide Hyperthermia Treatment, *Cancers*, vol. 14, no. 3, p. 625, (2022). https://doi.org/10.3390/cancers14030625
15. Song, C. W., Shakil, A., Osborn, J. L. & Iwata, K. Tumour oxygenation is increased by hyperthermia at mild temperatures. 1996, *Int J Hyperthermia*, vol. 25, no. 2, pp. 91 – 5, (2009). https://doi.org/10.1080/02656730902744171
16. Crezee, J., Oei, A. L., Franken, N. A. P., Stalpers, L. J. A. & Kok, H. P. Response: commentary: the impact of the time interval between radiation and hyperthermia on clinical outcome in patients with locally advanced cervical cancer. *Frontiers Oncol. Gen. Commentary Vol.* **10** https://doi.org/10.3389/fonc.2020.00528 (2020).
17. van Leeuwen, C. M. et al. A short time interval between radiotherapy and hyperthermia reduces in-field recurrence and mortality in women with advanced cervical cancer. *Radiat. Oncol.* **12** (1), 75. https://doi.org/10.1186/s13014-017-0813-0 (2017).
18. Crezee, H. et al. Thermoradiotherapy planning: integration in routine clinical practice. *Int J. Hyperthermia*, **32**, 1, pp. 41–49, 2016/01/02 2016, https://doi.org/10.3109/02656736.2015.1110757
19. Priester, M. I., Curto, S., van Rhoon, G. C. & Ten Hagen, T. L. M. External basic hyperthermia devices for preclinical studies in small animals. *Cancers (Basel)*. **13** (18). https://doi.org/10.3390/cancers13184628 (2021).
20. Salahi, S. et al. Miniature microwave applicator for murine bladder hyperthermia studies, *Int J Hyperthermia*, vol. 28, no. 5, pp. 456 – 65, (2012). https://doi.org/10.3109/02656736.2012.677931
21. Curto, S. et al. An integrated platform for small-animal hyperthermia investigations under ultra-high-field MRI guidance. *Int. J. Hyperth.* **34** (4), 341–351. https://doi.org/10.1080/02656736.2017.1339126 (2018).
22. Raaijmakers, E. A. L. et al. An MR-compatible antenna and application in a murine superficial hyperthermia applicator. *Int. J. Hyperth.* **34** (6), 697–703. https://doi.org/10.1080/02656736.2017.1369172 (2018).
23. Vicentini, M., Vassallo, M., Ferrero, R., Androulakis, I. & Manzin, A. In Silico evaluation of adverse eddy current effects in preclinical tests of magnetic hyperthermia. *Comput. Methods Programs Biomed.* **223**, 106975. https://doi.org/10.1016/j.cmpb.2022.106975 (Aug 2022).
24. Priester, M. I. et al. Preclinical Studies in Small Animals for Advanced Drug Delivery Using Hyperthermia and Intravital Microscopy, *Cancers*, vol. 13, no. 20, p. 5146, (2021). https://doi.org/10.3390/cancers13205146
25. Mahmood, J. et al. A Combination of Radiotherapy, Hyperthermia, and Immunotherapy Inhibits Pancreatic Tumor Growth and Prolongs the Survival of Mice, *Cancers*, vol. 12, no. 4, p. 1015, (2020). https://doi.org/10.3390/cancers12041015
26. Sebeke, L. C. et al. Visualization of thermal washout due to Spatiotemporally heterogenous perfusion in the application of a model-based control algorithm for MR-HIFU mediated hyperthermia. *Int. J. Hyperth.* **38** (1), 1174–1187. https://doi.org/10.1080/02656736.2021.1933616 (2021).
27. Zhu, L. et al. Targetability of cervical cancer by magnetic resonance-guided high-intensity focused ultrasound (MRgHIFU)-mediated hyperthermia (HT) for patients receiving radiation therapy. *Int. J. Hyperth.* **38** (1), 498–510. https://doi.org/10.1080/02656736.2021.1895330 (2021).
28. Kok, H. P. & Crezee, J. Hyperthermia treatment planning: clinical application and ongoing developments. *IEEE J. Electromagnet. RF Microwaves Med. Biology*. **5** (3), 214–222. https://doi.org/10.1109/jerm.2020.3032838 (2021).
29. Groen, J. A. et al. Robust, planning-based targeted locoregional tumour heating in small animals. *Phys. Med. Biol.* **69**, 085017. https://doi.org/10.1088/1361-6560/ad3324 (2024).
30. Myerson, R. J. et al. Components of a hyperthermia clinic: recommendations for staffing, equipment, and treatment monitoring. *Int. J. Hyperth.* **30** (1), 1–5. https://doi.org/10.3109/02656736.2013.861520 (2014).
31. Bruggmoser, G. et al. Guideline for the clinical application, Documentation and analysis of clinical studies for regional deep hyperthermia: quality management in regional deep hyperthermia. *Strahlenther. Onkol.* **188** (Suppl 2), 198–211. https://doi.org/10.1007/s00066-012-0176-2 (2012).
32. Paulsen, K. D., Geimer, S., Tang, J. & Boyse, W. E. Optimization of pelvic heating rate distributions with electromagnetic phased arrays. *Int. J. Hyperth.* **15** (3), 157–186. https://doi.org/10.1080/026567399285701 (1999).

33. Kok, H. P., de Greef, M., Borsboom, P. P., Bel, A. & Crezee, J. Improved power steering with double and triple ring waveguide systems: the impact of the operating frequency. *Int. J. Hyperth.* **27** (3), 224–239. https://doi.org/10.3109/02656736.2011.561270 (2011).
34. Canters, R. A., Paulides, M. M., Franckena, M., Mens, J. W. & van Rhoon, G. C. Benefit of replacing the Sigma-60 by the Sigma-Eye applicator. A Monte Carlo-based uncertainty analysis. *Strahlenther Onkol.* **189** (1), 74–80. https://doi.org/10.1007/s00066-012-0241-x (2013).
35. Hasgall, P. A. et al. It'is database for thermal and electromagnetic parameters of biological tissues, Version 4.1. https://doi.org/10.13099/VIP21000-04-1. Available online: https://itis.swiss/virtual-population/tissue-properties/database/dielectric-properties (2022).
36. Kok, H. P., Kotte, A. & Crezee, J. Planning, optimisation and evaluation of hyperthermia treatments. *Int. J. Hyperth.* **33**, 593–607. https://doi.org/10.1080/02656736.2017.1295323 (2017).
37. Weiland, T., Timm, M. & Munteanu, I. A practical guide to 3-D simulation. *IEEE Microw. Mag.* **9** (6), 62–75. https://doi.org/10.1109/Mmm.2008.929772 (2008).
38. Pennes, H. H. Analysis of tissue and arterial blood temperatures in the resting human forearm. *Journal Appl. Physiol. Article Vol.* **1** (2), 93–122 (1948).

Acknowledgements

The authors would like to thank Regiobouw Haarlemmermeer (Schiphol-rijk, Netherlands) for use of the infrared camera. We also thank Kemal Sumser and Flavia Liporace for assisting with dielectric property measurements.

Author contributions

Study concept and design: JAG, HPK, JC, RZ. Experimental work and data collection: JAG, RZ, JS. Data analysis: JG, RZ. Interpretation: JAG, HPK, JC, RZ. Figures: JAG. Manuscript preparation: JAG, HPK. Manuscript editing and reviewing: JAG, HPK, JC, HWML, MFB, RZ, JS, EMS. Funding: HPK, JC, MFB.

Funding

This study was supported by the Dutch Cancer Society KWF Kankerbestrijding, grant [2020–12985].

Declarations

Competing interests

J. Crezee and H.P. Kok have a research collaboration with Med-Logix srl. Med-Logix had no role in the study design, analyses, or interpretation of data, in the writing of the article, or in the decision to publish the results. M.F. Bijlsma has received research funding from Celgene, Frame Therapeutics, and Lead Pharma, and has acted as a consultant to Servier, Olympus and Wholomics. Other authors have no competing interest.

Additional information

Correspondence and requests for materials should be addressed to H.P.K.